Received: April 11, 2022. Revised: June 3, 2022. 162

International Journal of
Intelligent Engineering & Systems

http://www.inass.org/

Design A Super-Wideband MIMO Antenna for High Data Rate Systems

Hiwa Taha Sediq[1,2]* Javad Nourinia[1] Changiz Ghobadi[1] Nageb T. Rassam[3] Bahman Mohammadi[1]

[1]*Department of Electrical Engineering, Urmia University, Urmia, Iran*
[2]*Department of Information Technology, Shaqlawa Technical College, Erbil Polytechnic University, Erbil, Iraq*
[3]*Department of Information System Engineering,*
Engineering Technical College, Erbil Polytechnic University, Erbil, Iraq
* Corresponding author's Email: hiwa_eece@yahoo.com

Abstract: A novel cat-shaped patch multiple input multiple output (MIMO) antenna is discussed in this study for high data rate applications working with super wideband (SWB) systems. The single antenna is arranged by merging an elliptical geometric shape with a pair of compact triangular shapes. The designed unit cell dimensions are 26 mm x 24 mm. the single antenna operates from 2.23 to over 100 GHz and offers a bandwidth dimension ratio (BDR) of greater than 5567. This compact antenna is then used to design a MIMO antennas which consists of only two cat-shaped geometry without any decoupling structures. The similar antennas occupy an area of 26 x 50 mm^2 and the space between the geometric elements is 0.051 lower wavelength (λ_L). MIMO performance parameters are achieved by the antenna fabricated with low value mutual coupling characteristics, better channel capacity losses (CCL < 0.28 bits/s/Hz), envelope correlation coefficient (ECC < 0.003) by far-field radiation, and total active reflection coefficient (TARC ≤ −10 dB). The maximum peak gain value of 9.52 dB is attained from the proposed antenna, and the average values of radiation efficiency are more than 88%.

Keywords: MIMO antenna, Super-wideband, Cat-shaped patch, Error correlation coefficient, Mutual coupling.

1. Introduction

The design of antennas for moveable devices with improved radiation characteristics is very important for the development of technology in the field of wireless communication. The main significant principles for the novel propagation antenna are high data rate, compactness, efficiency, capacity, etc. The frequency spectrum of ultra-wideband applications is assigned for a range communication of 3.1-10.6 GHz by the federal communication commission (FCC) in 2002 [1-3]. A technical revolution has been made in the modified antennas technologies due to the continuous growth of ultra-wideband communications to satisfy the essential requirements of these prototyping systems [4]. Nevertheless, electromagnetic interference causes serious data delivery problems for UWB antennas. Therefore, the researchers have attempted to introduce a wider-bandwidth radio technology, called super wideband, to fulfill the demands of short-range and broadband communications. These antennas can be employed to transmit the audio, video, and data files even at a faster rate because of offering a high data rate and larger bandwidth. The main challenges that the designers considered while designing the planar SWB antennas are the high value of BDR, stable radiation pattern, and wide impedance bandwidth with less distortion at higher operating frequency. Hence, several investigators use different types of bandwidth optimization techniques such as: using coplanar waveguide (CPW) feed [5], modification in the patch radiating and the ground part [6,7], and other different feeding methods, like a tapered microstrip fed [8]. The fractal techniques are used to reduce the antenna size without affecting the impedance bandwidth range [9].

In order to increase the bandwidth of the octagonal ring-shaped design which operates from 2.59 to 31.14 GHz, a stub technique in the upper right corner of the radiating portion is used [7]. But sadly, this structure has big physical constraints and less-performance antennas. Researchers in [8] have designed a steering-shaped antenna for a super wideband monopole antenna powered by tapered microstrip. The antenna works from 2.3 to 34.8 GHz and the geometric ground plane is altered to partial rectangular shape with rounded corners to expand the antenna bandwidth, but the time domain study is essential to be examined in more detail. A good impedance bandwidth is provided from the study of [9] over the range of frequency-based third iterative fractal antenna for super wideband systems. Whereas, due to the large electrical dimensions of the antenna, it gives a low BDR value of 1605 and small gain results compared to the dimensions. Flexible antennas for sepur-wideband communications powered by CPW-fed were costructed to extend the operating range from 1.66 GHz to 56GHz [10], but the gain values of the designed antenna at all operating frequencies are less than 7 dBi.

In addition, with a frequency range of 2.9-40 GHz and a windmill-type decoupling structure, the [11] SWB antenna provides a good gain with larger electrical dimensions compared to the structure. The resource in [12] shows that a SWB antenna works in the range band of 3GHz to 20GHz. Exclusive designs are unacceptable for low bandwidth applications such as GSM, GPS, and Bluetooth because they relate to the aforementioned structure. High data rate applications were attained in [13] by reshaping the radiating spots and using the taper feed method to achieve a wide bandwidth. The antenna has some problems like detecting the physical capabilities of the SWB antenna when it receives a pulse and does not operate in a wide range of frequencies. Recently, Sharma et al. published an elliptical ring patch antenna with offset for SWB antennas [14]. The design offers a peak gain of 5.81 dBi with a bandwidth range (2.31-40 GHz), a BDR value of 1732, and a percentage bandwidth of 178. A clown-shaped patch antenna for SWB technology is indicated by [15] with an average gain of 6dBi and an equivalent bandwidth dimension ratio of 2768.

For wide-range communication, SWB radio technology can further improve high-speed data transmission by combining it with MIMO technology. Since this technology yields better interconnection network quality and diversity gain for various wireless communications. Correctly selecting signals in all directions can reduce the effect of deep fading. Therefore, at least one of the MIMO modulations needs to collect the spectrum in order to study the antenna diversity case. The electromagnetic interaction (mutual coupling) that occurs between the antenna elements is a significant topic in the design of MIMO antennas [16]. For this purpose, it is essential to propose MIMO diversity antennas with good isolation among array structures for broadband applications [17]. Maintaining low interconnectivity between the array elements without extra circuits gives the antenna excellent properties while designing MIMO antennas[18]. In order to enhance the high level of isolation and decrease the space between the antenna elements, various methods have been used, such as using electromagnetic bandgap (EBG) structures [19], designing a stub in the radiating ground part [20], changing the gap between the array radiators [21], implementing a decoupling structure in the ground part [22], introducing a stub among the radiation patches [23], and making a slit or using defected ground structure in the bottom plane [24].

Table 1. The proposed SWB antenna is compared with various listed antennas in dB and all gain* in dBi.

Ref.	Size [λ^2]	Frequency Range [GHz]	FBW [%]	BW Ratio:1	BDR	Gain [dB]
[7]	0.34 × 0.34	2.59-31.14	169	12.02	1461.9	5*
[8]	0.27 × 0.27	2.3-34.8	175.2	15.13	2403.3	7.21*
[9]	0.368×0.325	0.65-35.61	192	54.7	1605	6.5
[10]	0.188 × 0.138	1.66-56.1	195	33.7	7516	<7
[11]	0.56 × 0.56	2.9-40	172	13.7	2897	13.5*
[12]	0.3 × 0.3	3-20	147	6.6	1633	6
[13]	0.5×0.5	2.9-30	165	10.3	2894	6.2*
[14]	0.33 × 0.33	2.31-40	178	34.63	1732	5.81*
[15]	0:256 × 0:266	2.96- >100	>188	>33.78	>2768	-
Pro.	0.193 × 0.178	2.23- >100	>191	>44.84	>5567.6	9.52

The purpose of this article: First, to introduce a novel shape geometry for the SWB monopole antenna design. Second, the use of the noval single antenna to design the MIMO antenna for the SWB applications as described in the section 4. The structure of the unit cell antenna is combined from an elliptical model with two shaped triangles and a new notch printed on the radiation part. the partial ground plane of the proposed antenna is modifyed by making a triangular defect ground structure and two semi-circular strip-shaped slots. This modification provides a wide bandwidth of 2.23-100 GHz. The proposed single antenna is compared with other super wideband antennas reported as displayed in Table 1. As noticed, the supper wideband antenna has a small

Table 2. Novel layout antenna dimensions

Parameters	Ls	Ws	a	b	s	W_1	L_1
Dimensions (mm)	26	24	9	7.02	5.2	4.3	5.2
Parameters	W_3	L_3	x	n_1	m_1	b_s	b_r
Dimensions (mm)	4	0.2	3.6	8.67	3.11	7.47	2.95
Parameters	Lf	Wf	Lg	R	p	W_2	L_2
Dimensions (mm)	8.5	3.5	7.9	1.5	0.5	0.2	0.2
Parameters	L_4	sr	y	n_2	m_2	a_s	a_r
Dimensions (mm)	0.3	2.54	2.81	7.49	7.87	8.62	3.52

size and a wider impedance bandwidth than other existing super wideband antennas and even the proposed SWB antenna has a greater BDR value and characteristic gain compared to the described super wideband antennas.

2. Antenna design configuration

The structural antenna consists of an elliptical cat-shaped radiator and a half semi-elliptical ground part with a new notch load on the ground part. The geometric patch of the broad UWB antenna is collected by an ellipse adjacent to a pair of triangles as cat ears at the top radiation portion fed by the stripline, as shown in Fig. 1. Wide broadband is attained resulting in varying the position of the cat-shaped radiator's ears, printing novel slits on the patch, and etching the semi-elliptical slit on the partial ground plane. The dimensional layout of the configurational design is given detailly in Fig. 2. The dielectric material of the Rogers RT / Duroid 5880 is selected to design the structural substrate with a height (h) of 1.57 mm, a relative permittivity (εr) of 2.2, and a loss factor (δ) of 0.0009. The ANSYS simulation software (v17.2) is employed to analyze the major parameters of the designed antenna excited at 50ohms via a microstrip line. The dimensions of the planar antenna is $(24 \times 26 \times 1.57)\, mm^3$, and Table 2 shows the optimum dimensions for the proposed antenna.

2.1 Theoretical analysis

The Eq. (1) is employed to compute the lower frequency (F_L) of the structural antenna. By assisting the following equations, the net area of the novel geometrical radiation patch is computed for the monopole antenna. The standard Eq. (11) is used to calculate the constant value of the effective dielectric material (ε_{eff}). The lower cut-off frequency of 2.246 GHz is attained resulting in using the equations. The theoretically calculated F_L value is very close to the value obtained by the HFSS simulator.

$$F_L = \frac{c}{\lambda} = \frac{c}{2C\sqrt{\varepsilon_{eff}}}\ GHz \tag{1}$$

The patch effective area can be computed as, Area solid shapes – Area slot shapes

A) Area solid shapes (Ag) = A1 + A2 – A3 (2)

$$Area\ ellipse(A1) = \pi\, a\, b \tag{3}$$

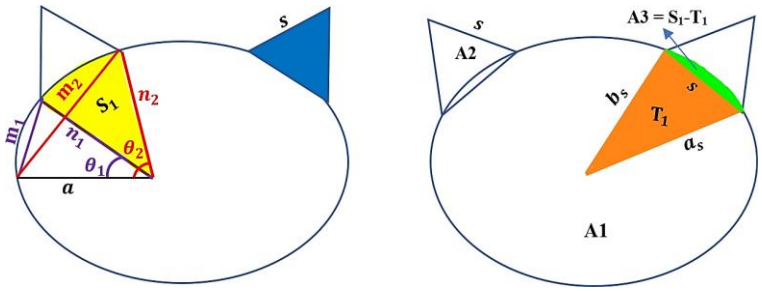

Figure. 1 Proposed structural antenna design

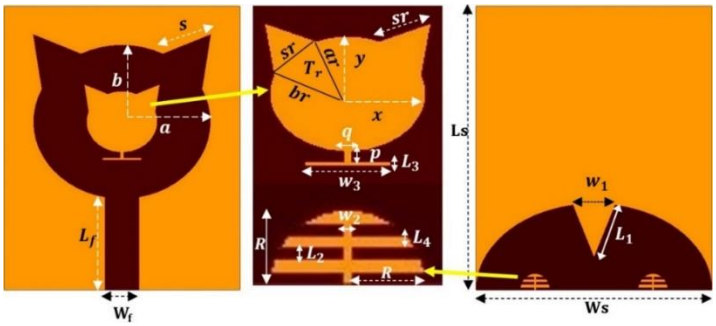

Figure. 2 Top and bottom views of the proposed cat-shaped antenna

$$Area\ triangle(A2) = \frac{\sqrt{3}}{4}\ s^2 \quad (4)$$

Area segment (A3) = Elliptical Sector (S_1) −Area triangle (T_1)

$$T_1 = \sqrt{H(H-a_s) - (H-b_s)(H-s)} \quad (5)$$

Where $= \frac{a_s+b_s+s}{2}$, $H_r = \frac{a_r+b_r+s_r}{2}$

$$S_1 = F(\theta_1) - F(\theta_2) \quad (6)$$

$$F(\theta) = \frac{a\,b}{2}\left(\theta - \tan^{-1}\left(\frac{(b-a)\sin(2\theta)}{b+a+(b-a)\cos(2\theta)}\right)\right)$$

$$\theta_1 = \cos^{-1}\left(\frac{a^2+{n_1}^2-{m_1}^2}{2a\,n_1}\right), \theta_2 = \cos^{-1}\left(\frac{a^2+{n_2}^2-{m_2}^2}{2a\,n_2}\right) \quad (7)$$

By using the values of Table 2 we get:

$$A3 = 20.28 - 19.3 = 0.98\ mm^2$$

$$\text{Ag} = \text{A1} + \text{A2} - \text{A3} = 219.95\ mm^2$$

B) Area slot shapes:

Area slot shapes (As) = elliptical slot + triangular slots - slot segments + first rectangular slot ($A4$) + second rectangular slot ($A5$)

$$T_r = \sqrt{H_r(H_r-a_r) - (H_r-b_r)(H_r-s_r)} \quad (8)$$

$$\theta_1 = \cos^{-1}\left(\frac{x^2+{ns_1}^2-{ms_1}^2}{2x\,ns_1}\right), \theta_2 = \cos^{-1}\left(\frac{x^2+{ns_2}^2-{ms_2}^2}{2x\,ns_2}\right) \quad (9)$$

where ns_1=3.52mm, ms_1=0.93mm; ns_2=2.95mm, ms_2=3.34mm and by using the values in the above equations we get:

$$A1 = \pi\ x\ y = 31.76\ mm^2$$

$$A2 = \frac{\sqrt{3}}{4}\ {s_r}^2 = 2.79\ mm^2$$

$$A3 = S_1 - T_r = 4.15 - 3.68 = 0.47\ mm^2$$

$$A4 = p \times q = 0.5 \times 0.4 = 0.2\ mm^2$$

$$A5 = L_3 \times w_3 = 0.2 \times 4 = 0.8\ mm^2$$

$$\text{As} = \text{A1} + 2 \times \text{A2} - 2 \times \text{A3} + \text{A4} + \text{A5}$$

$$\text{As} = 37.4\ mm^2$$

$$\text{Net Area of the geometry } (An) = \text{Ag} - \text{As}$$

$$An = 219.95 - 37.4 = 182.55\ mm^2$$

Now, the effective length of the semi-minor axis can be found as,

$$b_{eff} = \frac{An}{\pi\ a} = \frac{182.55}{3.14 \times 9} = 6.46\ mm \quad (10)$$

The circumference (C) of the Elliptical shape can be calculated via the following equations:

$$C = 2\pi\sqrt{\frac{a^2 + {b_{eff}}^2}{2}} = 49.22\ mm$$

By applying Eq (1), the lower frequency is attained as:

$$\varepsilon_{eff} = \frac{\varepsilon_r+1}{2} + \frac{\varepsilon_r-1}{2}[1 + 12\frac{h}{wf}]^{-\frac{1}{2}} \quad (11)$$

where c is free space speed and $\varepsilon_{eff} = 1.84$.

$$F_L = \frac{3 \times 10^{11}}{2 \times 49.22\ \times \sqrt{1.84}} = 2.246\ \text{GHz}$$

2.2 Antenna evolution procedure

Various modified iterations are made on the shape of the patch radiation and ground plane for the proposed cat-shaped design as displayed in Fig. 3. The solid-designed shape is linked to a transmission line without any slits to obtain super wideband antenna features in the situation of antenna I. The antenna operates in a notched band at 49.4 GHz with several resonant frequencies, whearas the impedance matching bandwidth of the SWB antenna is not very good over the entire frequency range because of rapid changes in impedance at the junction of the feeder and radiators. Therefore, a new slot is etched in the upper patch radiator to enhance the impedance bandwidth of the planar antenna in the second iteration (Antenna II). In that event, the level of the voltage standing wave ratio (VSWR) drops from 2.06 to 1.97 at 49.4 GHz and the antenna frequency range is extended from (2.29-49.4) GHz to (2.24- 49.9) GHz. In the third step, the antenna shape II is modified by adjoining a T-shaped slot at the bottom Cat-shaped notch and the VSWR value is improved to 1.74 as shown in Fig. 4. Besides, the lower cut-off frequency of is improved for the proposed antenna from 2.24GHz to 2.23GHz

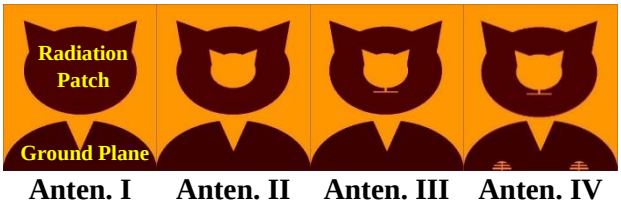

Figure. 3 Derivation stage of super wideband cat antenna

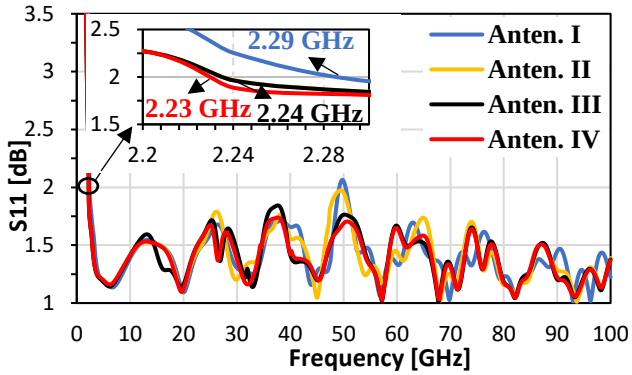

Figure. 4 Simulated S11 evaluation of the antenna

by printing a pair of the half-circular strip-shaped slot on the ground plane in the Antenna stage IV. The impedance bandwidth of the final geometry is also expanded to (2.23-100) GHz and even this stage decreases the VSWR value from 1.74 to 1.62 dB. Besides, the Bandwidth dimensional ratio (BDR) is also improved using iteration 4, as shown in Fig. 4. In conclusion, the proposed super wideband antenna has been acquired for multiple systems operating in the frequency band of S, C, X, Ku, K, Ka, V, and W in wireless communications. Due to broadband operation, this antenna can be also used for 5G radio applications.

3. Outcomes and discussion

This part describes experimental and simulation outcomes to better understand the performance of the proposed structure. So, the Cat-shaped SWB planner antenna is designed by using the parametric study listed in Table 2. Pictures of the manufactured prototype antenna joined to the SMA connector in the front and back views are exposed in Fig. 5. The ZVA67 device as a vector network analyzer (VNA) is applied to measure the antenna parameters. The designed antenna works well with the frequency spectrum of 2.23-100GHz, but due to the high frequencies limitation of vector network analyzers, the electronic devices can only measure data up to 67 GHz. A comparison between the measured and simulated VSWR of the super wideband antenna is plotted in Fig. 6. It is observed from the figure that the simulated outcome of the VSWR is proximity matched with the measured VSWR at the high-frequency spectrum from

(a) (b)

Figure. 5 Fabricated photo of the design with: (a) top and (b) bottom view of the antenna

20 to 67GHz. whereas, there is a minor deviation in the result from low operating frequency up to 20 GHz. This deviation may be due to the use of VNA cables, manufacturing tolerances, and the extended grounding effect of the SMA connector, which is not present in the simulation. The simulated results for VSWR begin at 2.23 GHz to 100 GHz and the measured VSWR results start at the operating frequency from 2.16 GHz to 67 GHz as shown in Fig. 6.

In the frequency range of 2.23-100GHz, the proposed antenna provides a good impedance bandwidth with a fractional bandwidth of 191.27 %, bandwidth ratio of 44.84:1, and a very high bandwidth dimension ratio of 5567.62. The results for the fabricated antenna covered an operating frequency of 2.16-67 GHz with a fractional bandwidth of 187.51% and BDR of 5458.17. The BDR value can be calculated by applying Eq. (12).

$$BDR = \frac{BW\%}{\lambda_{width} \times \lambda_{length}} \quad (12)$$

where λ_{length} and λ_{width} are the wavelength in terms of the lowest frequency.

Another important parametric study of the broadband antenna is the gain parameter. The simulated and measured realized gain values of the monopole structure are compared as plotted in Fig. 7. The gain curve becomes flat and has a small drop in the mid-frequency range due to the increased current at the sharp edges of the proposed structure. The maximum outcome of the simulated realized gain is 9.52 dB at 49.4 GHz. The measured value of the obtained gain fluctuates from 0.032 to 10.07 dB and the maximum experimental gain of the fabricated antenna is 10.07 dB at a frequency of 65.4GHz. The radiation efficiency with related to frequency varies from above 70 % to greater than 93 %. Fig. 7 depicts that the average achieved efficiency is above 88 % in the frequency range 2.23 GHz to 67 GHz.

4. MIMO antenna design

In order to certify good signal reception in a

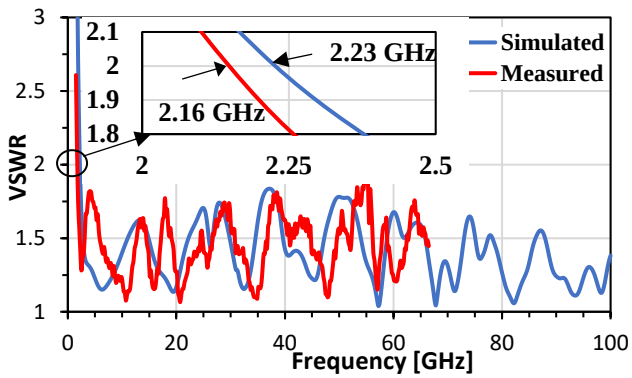

Figure. 6 Compared outcomes of measured and simulated VSWR

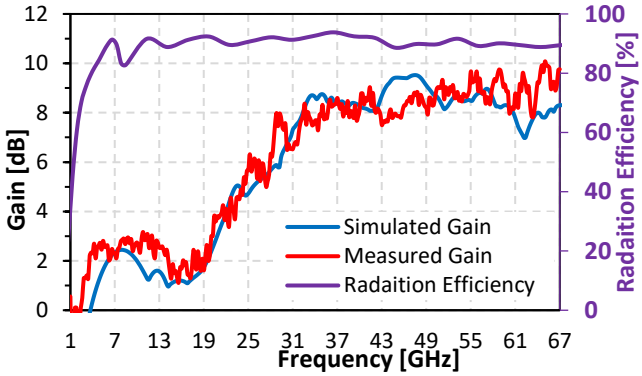

Figure. 7 Realized gain variation and radiation efficiency

multipath environment, a two-port diversity array is designed based on the proposed unit cell antenna. The monopole array consists of two unit cells that are placed orthogonally to feat the polarization diversity and decrease mutual coupling effect in the designed MIMO antenna system. The identical dual structure is separated by an electrical equivalent distance of $0.051\lambda_0$. The proposed MIMO antenna is printed on the same dielectric substrate (Rogers RT/Duroid 5880) as mentioned in the single antenna design. The equivalent electrical dimension of the super wideband MIMO antenna is $0.193\ \lambda_0 \times 0.371\lambda_0$ (26 x 50 mm^2) as shown in Fig. 8a. The proposed structural antenna is fabricated as a 2 x 2 MIMO antenna for short and wide range wireless communications as indicated in Fig. 8b.

The new MIMO monopole antenna is compared with other super wideband planar antennas described in the literature as given in Table 3. The comparison table shows that the size of the proposed MIMO planar antenna is smaller than the MIMO antennas reported in Ref. [16-24]. In addition, the dual-port antenna provides a wide operating frequency, large bandwidth ratio, less isolation, a small ECC value, and better gain compared with all references listed in the table. Moreover, the proposed MIMO antenna radiation efficiency of all researchers are shown in Table 3. As can be seen, the dual antenna has a high radiation efficiency percentage and the MIMO-SWB compated with only with two sractual elements.The tolerable diversity metrics attained for the MIMO-SWB planar make this compact antenna suitable for portable UWB, 5G, and all systems in the operating band S, C, X, Ku, K, Ka, V, and W.

5. MIMO characteristic measurement

5.1 Radiation pattern and current distribution

E ($\emptyset = 90^0$) and H plane (($\emptyset = 0^0$) are analyzed to explain the radiation patterns at resonance frequency of 3.5, 5, 20, 35, 50, and 65 GHz respectively. The automatic anechoic chamber is used to measure the radiation patterns of the proposed antenna, as exposed in Fig. 8c. The pattern is recorded at a rotation step of 5 degrees and the reference horn antenna is set to 2 meters. Fig. 9 estimates that the proposed radiation pattern from the antenna is the bidirectional pattern and the omnidirectional pattern for H-plane and E-plane, respectively. The simulation and measurement results are acceptable with minor differences in both cases from E and H planes. It is because of the environmental impacts from nearby devices, electromagnetic interference, and radiation influence from the antenna array elements.

Table 3. Compared characterizes of the proposed MIMO antenna with recent research antennas

[Ref.]	Size [mm^2]	Size [$\lambda_0{}^2$]	No. of elements	Frequency Range [GHz]	BW Ratio:1	Isolation (dB)	ECC	Gain	Efficiency (%)
[16]	40×80	0.59 × 1.19	2	4.5-8	1.78	>25	<0.002	4 dB	70
[17]	35 × 50	0.35 × 0.50	2	3–11	3.67	>25	0.004	<7 dB	>80
[18]	44×37	0.82×0.69	2	5.61–5.93	1.06	>24.5	<0.1	4 dB	-
[19]	33×48	0.22 × 0.32	2	2 -13.7	6.85	>20	<0.15	4.3 dBi	-
[20]	50×30	0.49×0.29	2	2.5-14.5	5.8	>20	<0.04	4.3 dB	-
[21]	93×47	0.96 × 0.48	2	3.1–10.6	3.42	>31	-	3.5 dBi	>70
[22]	44 × 22	0.38 × 0.19	2	2.53-2.66	1.05	38	<0.121	3.8 dBi	84
[23]	47.5 × 40	1.15 × 0.97	2	3.35-3.78	1.13	>20	<0.05	<4 dBi	<90
[24]	55 × 28	0.37 × 0.19	2	2.01–3.92	1.95	>15	0.01	<2 dB	<80
Pro.	26×50	0.193 × 0.371	2	2.23- >100	>44.84	>32	<0.0012	9.52 dB	93

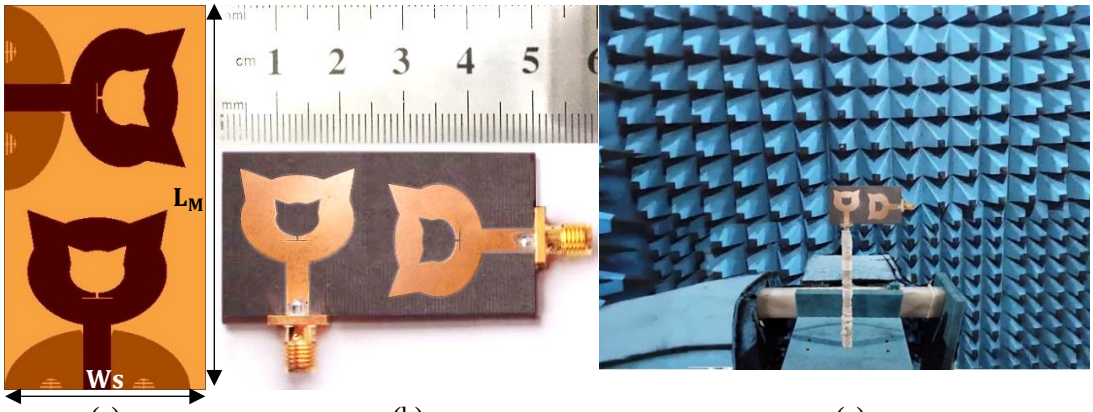

(a) (b) (c)

Figure. 8: (a) Layout and (b) Fabricated prototype of the proposed MIMO antennas with (c) Photo lab. of the radiation pattern in the anechoic chamber

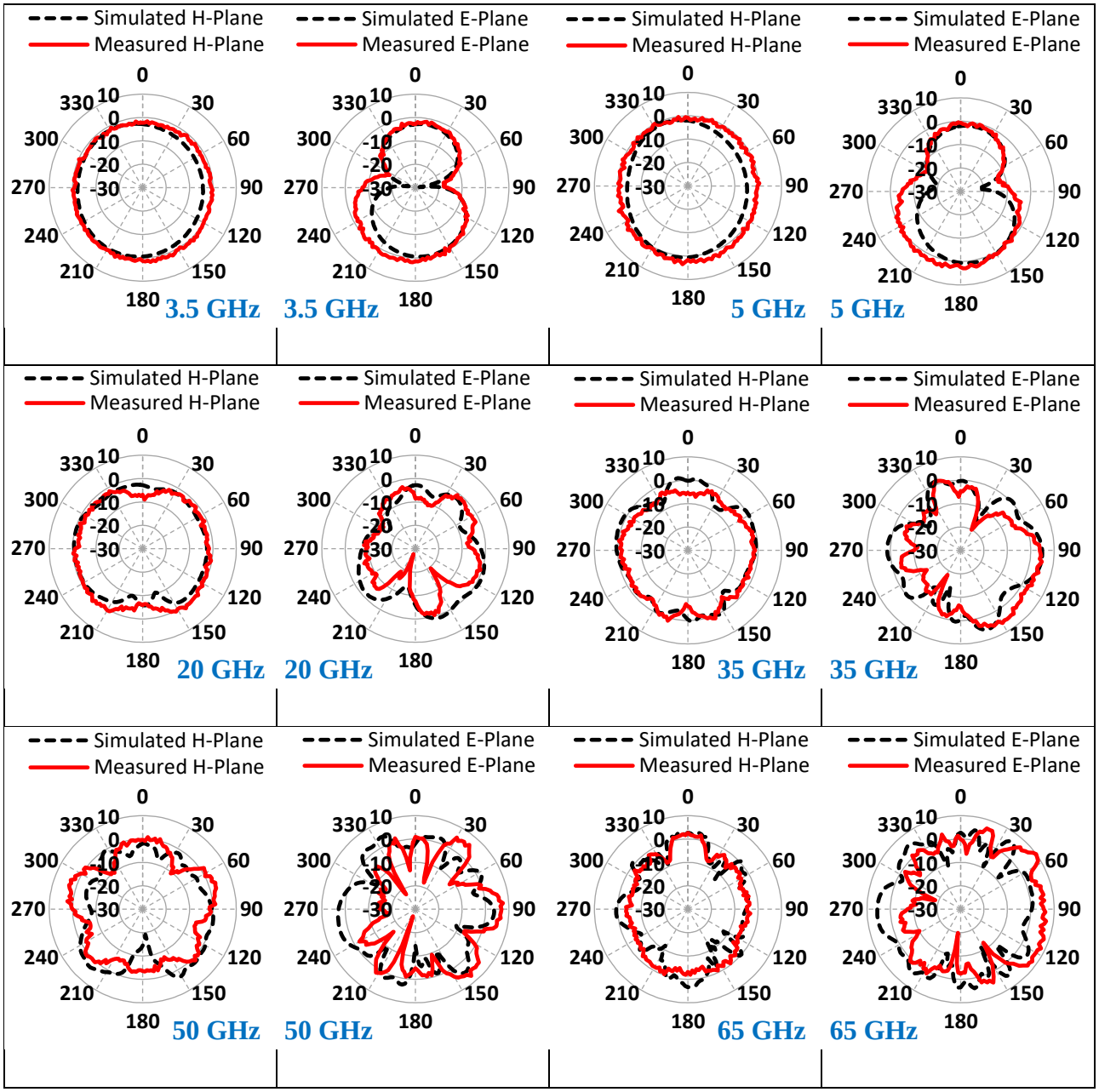

Figure. 9 Far-field radiation pattern simulated and measured at frequency of (3.5, 5, 20, 35, 50, and 65) GHz for E and H plane

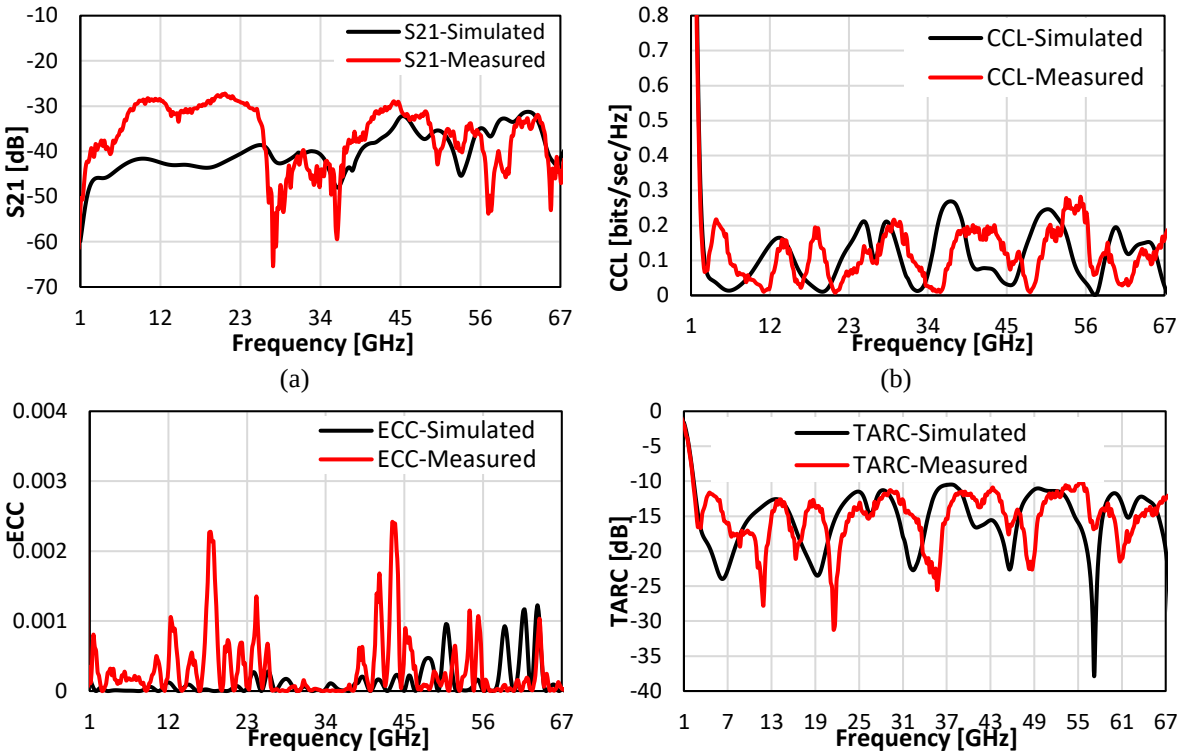

Figure. 10 Measured and simulated results of: (a) S_{21}, (b) CCL, (c) ECC, and (d) TARC

5.2 Isolation

Isolation is a significant property of MIMO antennas because this property reveals the mutual coupling effects between antenna structures [25]. It is found from Fig. 10a that for all operating frequency range, the mutual coupling between the antenna elements is lower than -32 dB and almost equal to -28 dB for the simulated part and measured part respectively. Therefore, planar MIMO antennas provide better isolation between the ports in the designed structure. The S_{21} value of the 2-port structure is found using Eq. (13).

$$Isolation = -10\, log10[S12^2]\ dB \tag{13}$$

5.3 Channel capacity loss

An extra significant parametric study among array antennas for a MIMO planer antenna is the channel capacity loss. This parameter is analyzed and the measured and simulated results of CCL for the proposed system is illustrated in Fig. 10b. It is recommended that the CCL value be less than 0.4 bps/Hz. It can be seen that across operational bandwidth, the CCL results are less than 0.26 and 0.28 bps /Hz in the simulated and measured cases, respectively. These outcomes demonstrate that the CCL property of the designed antenna is a very good candidate and has better throughput for MIMIO-SWB systems. Eq. (14) is used to calculate the value of this parameter.

$$CCL = -log_2\, det(\varphi^R) \tag{14}$$

where φ^R is the correlation matrix reception antenna.

5.4 Envelope correlation coefficient

The correlation coefficient (ECC) parameter is responsible for describing the correlation between channels of MIMO antennas. The envelope correlation coefficient can be represented in Eq. (15) using the S-parameters (S11, S12, S22, and S21). The proper value of ECC should be less than 0.5 in practical application. However, the resulting ECC for the proposed structure is below 0.0025 in simulation and measurement for the entire region. Fig. 10c illustrates the comparison between measured and simulated ECC outcomes for the proposed 2 × 2 structure.

$$ECC = \frac{|S^*_{11}S_{12}+S^*_{21}S_{22}|^2}{(1-(|S_{11}|^2+|S_{21}|^2))(1-(|S_{22}|^2+|S_{12}|^2))} \tag{15}$$

5.5 Total active reflection coefficient

A new parameter, known as TARC, is used to study the MIMO characteristics. This parameter has

the ability to indicate changes in the mutual and self-impedances of the array antennas. The accepted value of TARC is practically less than or equal to 0 dB. In this investigation, the measured and simulated results of TARC are below −10 dB in the entire range of both the proposed structure results as illustrated in Fig. 10d. The TARC results are found using standard Eq. (16) regarding the S-parameters (S11, S12, S22, and S21).

$$TARC = \sqrt{\frac{\left|S_{11}+S_{12}e^{j\theta}\right|^2+\left|S_{21}+S_{22}e^{j\theta}\right|^2}{2}} \quad (16)$$

6. Conclusion

This study presents a new cat-shaped antenna for SWB applications. The single SWB antenna operates in the frequency range from 2.23 GHz to over 100 GHz. The proposed antenna provides a maximum bandwidth ratio of 44.84:1, fractional bandwidth of 191 %, high BDR of 5567 and large gain of 9.52 dB. Besides, using this compact antenna to design 2 × 2 MIMO antennas are presented. The measurement and simulation results of radiation pattern, isolation, CCL, ECC, TARC, and MEG are compared with their stander values. The acceptable diversity metrics obtained for the MIMO-SWB planar make this compact antenna suitable for portable UWB, 5G, and all systems in the operating band S, C, X, Ku, K, Ka, V, and W. The authors are working to reduce the size of the MIMO antenna in the future to provide better convenience for use in microwave applications.

Conflicts of interest

"The authors declare no conflict of interest."

Author contributions

H. T. Sediq carried out the design of the antenna scheme, performed the experiments, and wrote the manuscript. J. Nourinia and Ch. Ghobadi supervised and reviewed the manuscript. N. T. Rassam helped in drafting the manuscript. B. Mohammadi guided the work and supervised the experimental design. All authors read and approved the final manuscript.

References

[1] H. T. Sediq, J. Nourinia, C. Ghobadi, F. Alizadeh, A. Lalbakhsh, and B. Mohammadi, "UWB Dual-notched Planar Antenna by Incorporating Single Compact EBG", *In Photonics and Electromagnetics Research Symposium (PIERS)*, Hangzhou, China, pp. 700-704, 2021.

[2] N. A. Jan, S. H. Kiani, D. A. Sehrai, M. R. Anjum, A. Iqbal, M. Abdullah, and S. Kim, "Design of a compact monopole antenna for UWB applications", *CMC COMPUTERS MATERIALS & CONTINUA*, Vol. 66, No. 1, pp. 35-44, 2021.

[3] H. T. Sediq, "Design of ultra-wideband dipole antenna for WiMAX wireless applications", *Polytechnic Journal*, Vol. 8, No. 3, pp. 13-25, 2018.

[4] S. Lakrit, S. Das, S. Ghosh, and B. T. P. Madhav, "Compact UWB flexible elliptical CPW-fed antenna with triple notch bands for wireless communications", *International Journal of RF and Microwave Computer-Aided Engineering*, Vol. 30, No. 7, p. e22201, 2020.

[5] H. T. Sediq and Y. N. Mohammed, "Performance analysis of novel multi-band monopole antenna for various broadband wireless applications", *Wireless Personal Communications*, Vol. 112, No. 1, pp. 571-585, 2020.

[6] H. T. Sediq, J. Nourinia, C. Ghobadi, and B. Mohammadi, "A Novel Eye-shaped Monopole Antenna for Wideband and 5G Applications", *IETE Journal of Research*, pp. 1-11, 2020.

[7] T. Okan, "A compact octagonal-ring monopole antenna for super wideband applications", *Microwave and Optical Technology Letters*, Vol. 62, No. 3, pp. 1237-1244, 2020.

[8] S. Alluri and N. Rangaswamy, "Compact high bandwidth dimension ratio steering-shaped super wideband antenna for future wireless communication applications", *Microwave and Optical Technology Letters*, Vol. 62, No. 12, pp. 3985-3991, 2020.

[9] S. Singhal and A. K. Singh, "Elliptical monopole based super wideband fractal antenna", *Microwave and Optical Technology Letters*, Vol. 62, No. 3 , pp. 1324-1328, 2020.

[10] M. R. Hasan, M. A. Riheen, P. Sekhar, and T. Karacolak, "Compact CPW-fed circular patch flexible antenna for super-wideband applications", *IET Microwaves, Antennas & Propagation*, Vol. 14, No.10, pp. 1069-1073, 2020.

[11] C. Yu, S. Yang, Y. Chen, W. Wang, L. Zhang, B. Li, and L. Wang, "A super-wideband and high isolation MIMO antenna system using a windmill-shaped decoupling structure", *IEEE Access*, Vol. 8, pp. 115767-115777, 2020.

[12] M. Elhabchi, M. N. Srifi, and R. Touahni, "A novel modified U-shaped microstrip antenna for super wide band (SWB) applications", *Analog Integrated Circuits and Signal Processing*, Vol. 102, pp. 571–578, 2020.

[13] A. V. Boologam, K. Krishnan, S. K. Palaniswamy, C. T. Manimegalai, and S. Gauni, "On the Design and Analysis of Compact Super-Wideband Quad Element Chiral MIMO Array for High Data Rate Applications", *Electronics*, Vol. 9, No. 12, p. 1995, 2020.

[14] V. Sharma, J. K. Deegwal, and D. Mathur, "Super-Wideband Compact Offset Elliptical Ring Patch Antenna for 5G Applications", *Wireless Personal Communications*, Vol. 122, No. 2, pp. 1655-1670, 2022.

[15] R. K. Garg, S. Singhal, and R. Tomar, "A CPW Fed Clown-Shaped Super Wideband Antenna", *Progress In Electromagnetics Research Letters*, Vol. 99, No. 00, pp. 159-168, 2021.

[16] A. H. Jabire, H. X. Zheng, A. Abdu, and Z. Song, "Characteristic mode analysis and design of wide band MIMO antenna consisting of metamaterial unit cell", *Electronics*, Vol. 8, No. 1, p. 68, 2019.

[17] L. Wang, Z. Du, H. Yang, R. Ma, Y. Zhao, X. Cui, and X. Xi, "Compact UWB MIMO antenna with high isolation using fence-type decoupling structure", *IEEE Antennas and Wireless Propagation Letters*, Vol. 18, No. 8, pp. 1641-1645, 2019.

[18] A. Iqbal, O. A Saraereh, A. Bouazizi, and A. Basir, "Metamaterial-based highly isolated MIMO antenna for portable wireless applications", *Electronics*, Vol. 7, No. 10, p. 267, 2018.

[19] A. Altaf, A. Iqbal, A. Smida, J. Smida, A. A. Althuwayb, S. H. Kiani, M. Alibakhshikenari, F. Falcone, and E. Limiti, "Isolation improvement in UWB-MIMO antenna system using slotted stub", *Electronics*, Vol. 9, No. 10, p. 1582, 2020.

[20] A. Iqbal, O. A. Saraereh, A. W. Ahmad, and S. Bashir, "Mutual coupling reduction using F-shaped stubs in UWB-MIMO antenna", *IEEE Access*, Vol. 6, pp. 2755-2759, 2018.

[21] A. H. Radhi, R. Nilavalan, Y. Wang, H. S. A. Raweshidy, A. A. Eltokhy, and N. A. Aziz, "Mutual coupling reduction with a wideband planar decoupling structure for UWB–MIMO antennas", *International Journal of Microwave and Wireless Technologies*, Vol. 10, No. 10, pp. 1143-1154, 2018.

[22] H. Islam, S. Das, T. Ali, P. Kumar, S. Dhar, and T. Bose, "Split Ring Resonator-Based Bandstop Filter for Improving Isolation in Compact MIMO Antenna", *Sensors*, Vol. 21, No. 7, p. 2256, 2021.

[23] C. Wang, X. S. Yang, and B. Z. Wang, "A metamaterial-based compact broadband planar monopole MIMO antenna with high isolation", *Microwave and Optical Technology Letters*, Vol. 62, No. 9, pp. 2965-2970, 2020.

[24] A. K. Biswas and U. Chakraborty, "Reduced mutual coupling of compact MIMO antenna designed for WLAN and WiMAX applications", *International Journal of RF and Microwave Computer-Aided Engineering*, Vol. 29, No. 3, p. e21629, 2019.

[25] H. T. Sediq, J. Nourinia, and C. Ghobadi, "A Novel Shaped Antenna for Designing UWB-MIMO System in Microwave Communications", *AEU-International Journal of Electronics and Communications*, p. 154249, 2022.